NASA/CR–2012-216039

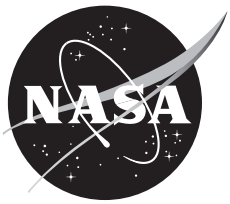

Determination of HART I Blade Structural Properties by Laboratory Testing

Sung N. Jung
Konkuk University
Seoul, South Korea

Benton H. Lau
Ames Research Center
Moffett Field, California

August 2012

The NASA STI Program Office . . . in Profile

Since its founding, NASA has been dedicated to the advancement of aeronautics and space science. The NASA Scientific and Technical Information (STI) Program Office plays a key part in helping NASA maintain this important role.

The NASA STI Program Office is operated by Langley Research Center, the Lead Center for NASA's scientific and technical information. The NASA STI Program Office provides access to the NASA STI Database, the largest collection of aeronautical and space science STI in the world. The Program Office is also NASA's institutional mechanism for disseminating the results of its research and development activities. These results are published by NASA in the NASA STI Report Series, which includes the following report types:

- TECHNICAL PUBLICATION. Reports of completed research or a major significant phase of research that present the results of NASA programs and include extensive data or theoretical analysis. Includes compilations of significant scientific and technical data and information deemed to be of continuing reference value. NASA's counterpart of peer-reviewed formal professional papers but has less stringent limitations on manuscript length and extent of graphic presentations.

- TECHNICAL MEMORANDUM. Scientific and technical findings that are preliminary or of specialized interest, e.g., quick release reports, working papers, and bibliographies that contain minimal annotation. Does not contain extensive analysis.

- CONTRACTOR REPORT. Scientific and technical findings by NASA-sponsored contractors and grantees.

- CONFERENCE PUBLICATION. Collected papers from scientific and technical conferences, symposia, seminars, or other meetings sponsored or cosponsored by NASA.

- SPECIAL PUBLICATION. Scientific, technical, or historical information from NASA programs, projects, and missions, often concerned with subjects having substantial public interest.

- TECHNICAL TRANSLATION. English-language translations of foreign scientific and technical material pertinent to NASA's mission.

Specialized services that complement the STI Program Office's diverse offerings include creating custom thesauri, building customized databases, organizing and publishing research results . . . even providing videos.

For more information about the NASA STI Program Office, see the following:

- Access the NASA STI Program Home Page at *http://www.sti.nasa.gov*

- E-mail your question via the Internet to help@sti.nasa.gov

- Fax your question to the NASA Access Help Desk at (301) 621-0134

- Telephone the NASA Access Help Desk at (301) 621-0390

- Write to:
  NASA Access Help Desk
  NASA Center for AeroSpace Information
  7115 Standard Drive
  Hanover, MD 21076-1320

NASA/CR–2012-216039

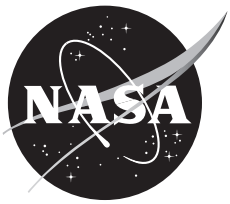

Determination of HART I Blade Structural Properties by Laboratory Testing

Sung N. Jung
Konkuk University
Seoul, South Korea

Benton H. Lau
Ames Research Center
Moffett Field, California

National Aeronautics and
Space Administration

Ames Research Center
Moffett Field, California 94035-1000

August 2012

Acknowledgments

The measurement of HART I blade properties began by Benton Lau in late 2005 under U.S.–German MOU (Memorandum of Understanding). Much of the measurements were finished, but the study was never completed due to a serious health issue for Benton Lau. He passed away in 2010. Later, Professor Sung Jung at Konkuk University of South Korea proposed research on HART I- and HART II-related activities using his sabbatical leave for one year. He joined Ames Research Center in September 2011 and resumed the blade property measurement, leading to the successful documentation of the test data. He was supported by a leading foreign research institute recruitment program through the National Research Foundation of Korea (NRF), funded by the Ministry of Education, Science, and Technology (MEST) (K2060100001). The authors wish to thank Berend van der Wall of the German Aerospace Center (DLR) for providing HART I blades, Brandon Hagerty for doing preliminary measurements, Wayne Johnson and William Warmbrodt of Ames Research Center, Joon Lim and Thomas Maier of AFDD (U.S. Army Aeroflightdynamics Directorate) for valuable comments and support, and Eduardo Solis of Ames Research Center for artwork on figures.

Available from:

NASA Center for AeroSpace Information
7115 Standard Drive
Hanover, MD 21076-1320
(301) 621-0390

National Technical Information Service
5285 Port Royal Road
Springfield, VA 22161
(703) 487-4650

TABLE OF CONTENTS

LIST OF FIGURES

LIST OF TABLES

NOMENCLATURE

BVI	=	blade-vortex interaction
c	=	blade chord
CAMRAD	=	Comprehensive Analytical Model of Rotorcraft Aerodynamics and Dynamics
CG	=	center of gravity
DEI	=	Dynamic Engineering, Inc.
DLR	=	German Aerospace Center
DNW	=	German–Dutch wind tunnel
EA	=	elastic axis
EI_{CHD}	=	chord bending stiffness
EI_{FLAP}	=	flap bending stiffness
GJ	=	torsion stiffness
HART	=	Higher Harmonic Control Aeroacoustic Rotor Test
HHC	=	higher harmonic control
I_P, I_θ	=	polar mass moment of inertia
k_P	=	polar radius of gyration
MOI	=	moment of inertia
ONERA	=	Office National d'Études et de Recherches Aérospatiales
QC	=	quarter chord
R	=	rotor radius
RPM	=	revolutions per minute
SI	=	International System of Units
Y, Z	=	blade section coordinates
Ω	=	rotor speed
Ω_0	=	rotor nominal speed

DETERMINATION OF HART I BLADE STRUCTURAL PROPERTIES BY LABORATORY TESTING

Sung N. Jung[1] and Benton H. Lau

Ames Research Center

SUMMARY

The structural properties of Higher Harmonic Control Aeroacoustic Rotor Test (HART I) blades were measured using the original set of blades tested in the German–Dutch wind tunnel (DNW) in 1994. The measurements include bending and torsion stiffness, geometric offsets, and mass and inertia properties of the blade. The measured properties were compared to the estimated values obtained initially from the blade manufacturer. The previously estimated blade properties showed consistently higher stiffness, up to 30 percent for the flap bending in the blade inboard root section. The measured offset between the center of gravity and the elastic axis is larger by about 5 percent chord length, compared to the estimated value. The complete structural properties of HART I blades were obtained using the present measured data along with the previously available data provided by the blade manufacturer. The rotor structural dynamics analysis in vacuum condition was also carried out to examine the validity of the measured blade properties.

INTRODUCTION

In 1994, the Higher Harmonic Control Aeroacoustic Rotor Test (HART I) was conducted in an open-jet anechoic test chamber of the German–Dutch wind tunnel (DNW) by a joint research team from the German Aerospace Center (DLR), the French Office National d'Études et de Recherches Aérospatiales (ONERA), NASA Langley, DNW, and the U.S. Army (ref. 1). The main focus of the task was to measure the noise level, airloads, vortex wake, and blade motions of a rotor in various flight conditions, with and without higher harmonic control (HHC) pitch inputs, with objectives to improve the physical understanding of the blade-vortex interaction (BVI) phenomena and to promote the HHC techniques for active rotor control. The test data included extensive acoustic and vortex flow measurements that resulted in a milestone accomplishment in rotorcraft aeromechanics (ref. 2).

The HART I rotor is a four-bladed, Mach-scaled model of the BO-105 hingeless main rotor. The blades are composed of E-glass spar and honeycomb materials and were manufactured by Dynamic Engineering, Inc. (DEI) in the early 1990s. Even though some of the measured properties such as the nonrotating blade frequencies are available, the actual blade properties were never measured as a complete set. Previous studies on the validation of the HART I rotor (refs. 3–6) indicate that the predicted airloads are reasonably matched with the measured data, whereas the structural load results

[1] Department of Aerospace Information Engineering, Konkuk University, Seoul, South Korea

exhibit poor correlation with the wind tunnel test data, in terms of both magnitude and phase. In some investigations, good correlation was obtained by adjusting the blade stiffness and inertia (refs. 5, 6). This suggests uncertainty in the blade property set, and there is a need for reliable HART I blade properties that can only be achieved by a careful measurement process. Furthermore, it is known that up to four different sets of blade property data for HART I have been in use, and there is a clear need for a unified version of the blade properties.

In an attempt to resolve the uncertainty issue associated with the HART I blade properties and to provide the required data set to the rotorcraft community, the blades used in the wind tunnel test in 1994 were delivered to NASA Ames Research Center in 2005 from the DLR. Since then, a series of laboratory tests have been conducted to experimentally determine the structural properties of HART I blades. The measurements include geometric offsets, bending and torsion stiffness, and mass and inertia properties. In order to ensure the reliability of the measured data, multiple testing techniques were introduced for specific blade properties. These test techniques include the mirror method (ref. 7) and 3-point bending (ref. 8) for stiffness properties, as well as the trifilar (ref. 9) and pendulum methods (ref. 10) for inertia properties.

This report documents the measurement of the blade properties and provides a complete set of measurement data for HART I blades. The measurement methods and test procedures adopted for specific properties are described along with the detailed measured records.

HART I ROTOR

The HART I rotor is a four-bladed, 40-percent Mach-scaled hingeless BO-105 model with 2 m radius and 0.121 m chord length. The geometric properties of HART I blades are summarized in table 1. Figure 1 shows the detailed dimensions measured for the HART I blade, which has an overall span length of 1.873 m from root to tip. The reference blade (blade 1) is heavily equipped with pressure transducers and strain gauges distributed along the span and chord. Because of these sensors, the weight of blade 1 is about 6 percent heavier than the other blades. The weights of individual HART I blades are documented in the test report (ref. 11). Most of the pressure sensors are installed at three radial stations (r/R = 0.75, 0.87, 0.97) to obtain the complete pressure distribution along the chordwise direction. A total of 32 strain gauges, distributed between r/R = 0.14 and 0.83, are attached on the blade surface to measure the structural loads and the elastic deflections of the blade. Figure 2 shows the configuration of the HART I rotor hub. All four HART I blades are identified with different colors. For instance, the instrumented blade is identified with yellow ribbons taped in the blade root region and named briefly as H1Y. The rest of the blades are named in a similar manner as shown in table 2. The additional blade H1S (spare) is also available for the structural test.

HART I BLADE PROPERTY MEASUREMENT

Ideally, the instrumented blade (blade 1) would be used to measure the blade structural properties because most of the wind tunnel measurements were carried out using blade 1. However, blade 1 was severely damaged during a separate test after HART I and, consequently, could not be used for

further structural tests. The other blades also suffer from partial damage concentrating mostly near the trailing edge of the blades' inboard region. In general, they appear appropriate for structural tests because the primary load carrying parts remain relatively healthy despite the accident. Therefore, measurements were made using the remaining set of blades. In addition, a spare HART I blade (H1S), which remains clean and intact, is available for the structural tests. One of the HART I blades (blade 3, H1B) was cut into several pieces to obtain the mass and inertia properties of the blade cross sections. As is shown in figure 1, the airfoil section of the HART I blade with constant chord starts at 22 percent radial station (0.22R) up to the tip of the blade. For convenience, inboard of 0.22R is called the blade root section, and the outboard portion is called the blade uniform section. Specific testing methods and procedures for the measurement of HART I blade properties are described in the following section.

TABLE 1. GENERAL PROPERTIES OF THE HART I BLADE

Rotor radius, m	2.0
Blade chord, m	0.121
Airfoil	NACA 23012mod
Blade root cutout, m	0.44
Blade twist, deg	–8.0
Blade twist at the tip, deg	–2.4
Position of zero twist, m	1.4
Airfoil tab length, m	0.0054
Airfoil tab thickness, m	0.0008

TABLE 2. HART I BLADE NAMES

Blade No.	**Nickname**
Blade 1	H1Y (yellow)
Blade 2	H1G (green)
Blade 3	H1B (blue)
Blade 4	H1R (red)
Spare blade 1	H1S (spare)

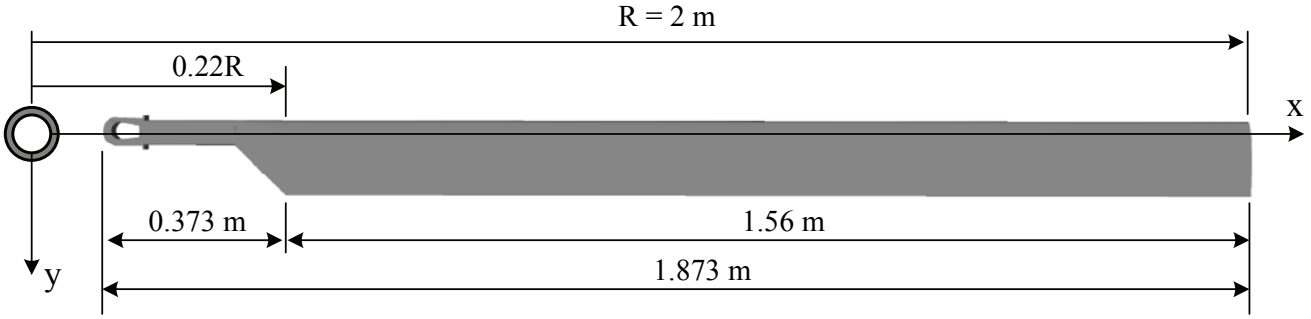

Figure 1. Geometric dimensions measured for the HART I blade.

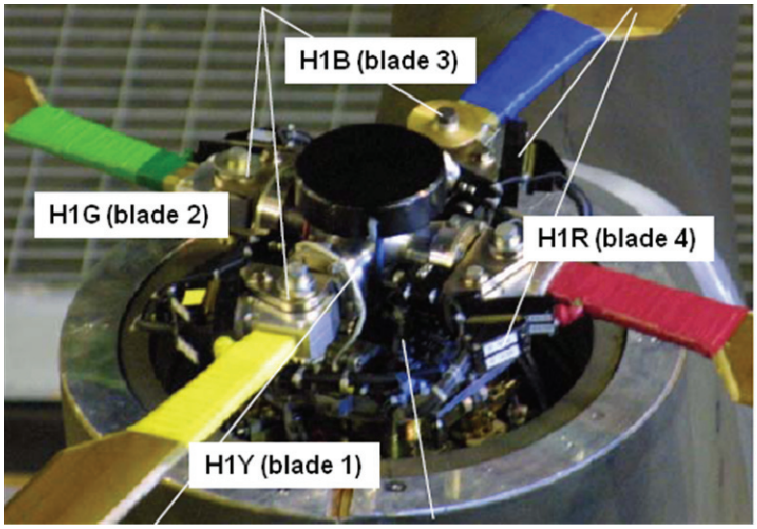

Figure 2. Configuration of the HART I rotor hub.

Mass and Inertia Properties

Blade 3 (H1B) was cut into six small pieces to measure the mass and inertia properties of the blade uniform section. Figure 3 shows the schematic view of the cut-out sections. The region of the cut sections is about 994 mm (39.125 in.) long, starting from the blade tip. As shown in figure 3, they consist of three 12.7-mm-wide sections (A, B, E), two 25.4-mm-wide sections (C, F), and one 905-mm-wide section (D). The actual dimensions of the cut-out sections indicate some scatter due to imperfections in the blade cuts. The weights of each blade section segment were measured using a mechanical balance. Table 3 shows the mass properties of individual sections. The blade tip sections (A, B) have a large piece of metal near the leading edge resulting in about twice as much weight compared to the other sections. The chordwise center of gravity (CG) is measured by placing the blade section segments on a needle top, as shown in figure 4. The stable position of a section is marked by the painted tip of the needle top and then the distance from the leading edge is measured. This process is repeated several times to reduce the measurement error. The position of CG in the chordwise direction varies between the sections because of the differences in the internal layouts (e.g., balancing weights and internal cables), as well as the uncertainty in the cuts. The mid-section D has relatively uniform properties with significantly less uncertainty in geometries and layouts. It is finally determined that the measured CG of the blade uniform section is located at 26.5 percent chord from the leading edge of the blade section.

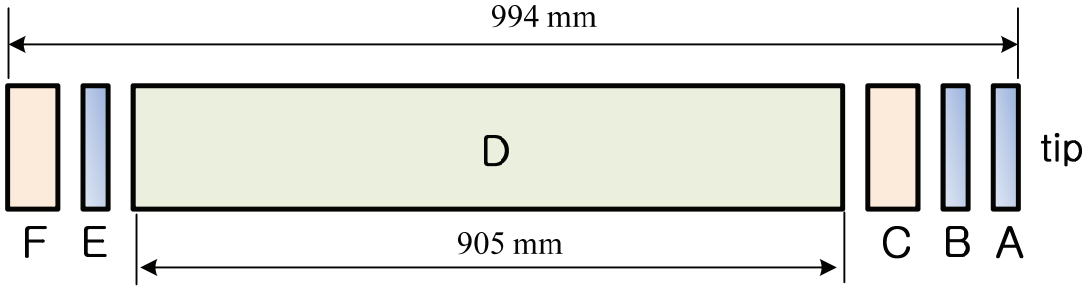

Figure 3. Schematic view for cut-out sections of H1B (blade 3).

TABLE 3. MASS PROPERTIES OF H1B CUT SECTIONS

Section	Actual Width, mm	Weight, kg	Polar MOI at QC, kg-m
A	12.7	0.0260	0.000670
B	13.5	0.0349	–
C	25.9	0.0311	0.000534
D	905	0.8677	0.000572
E	13.1	0.0135	–
F	26.2	0.0269	0.000697

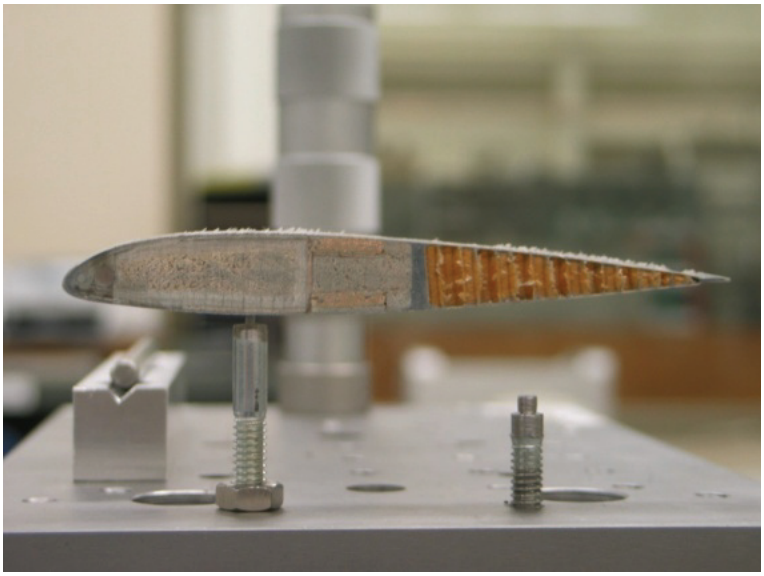

Figure 4. Measurement of the chordwise center of gravity.

The polar mass moment of inertia (MOI) is obtained using a trifilar pendulum method (ref. 9). In this method, a circular disk with known weight and inertia is suspended by three thin cables having equal lengths (see fig. 5). The polar MOI I_θ is obtained using the relationship given by (ref. 9):

$$I_\theta = \frac{1}{b}\frac{W r^2 t^2}{4\pi^2 l_c} \tag{1}$$

where W is the weight of the suspended object, r is the radial distance of the cable attachment from the disk center, t is the time period, l_c is the length of the cable, and b is the length of the blade segment. The measurement is carried out in the following sequence: 1) place the blade uniform section on the suspended disk; 2) start a pendulum motion with a small initial angle; 3) obtain the period of oscillations after sufficient number of cycles; and 4) repeat the above procedures for an

averaged response. Figure 5 shows a photograph taken for the actual measurement on the polar MOI of a blade uniform section. The circular disk has a weight of 0.476 kg with a diameter of 0.3048 m. The disk is supported by three cables having the dimension of 0.5733 m and the radius of 0.146 m from the center. A laser sensor and a frequency counter (HP 5334B) are used to measure the period of oscillations. About 40 cycles are repeated for each section to obtain the frequency response. Table 4 shows the raw data on measured periods of oscillations for sections A, C, D, and F. The actual inertia component is obtained using Eq. (1) after subtracting the contribution of the circular disk. The measured polar MOI for each section is presented in table 3. It is noted that the measurement is made at the quarter chord (QC) axis of the blade sections. The polar MOI at CG and EA (elastic axis) is evaluated respectively using the parallel axis theorem as given by,

$$I_{\theta,CG} = I_{\theta,QC} - md_1^2$$
$$I_{\theta,EA} = I_{\theta,QC} - m(d_1^2 - d_2^2) \tag{2}$$

where m denotes the mass of the sections, d_1 is the chordwise offset between CG and QC, and d_2 is the chordwise offset between CG and EA.

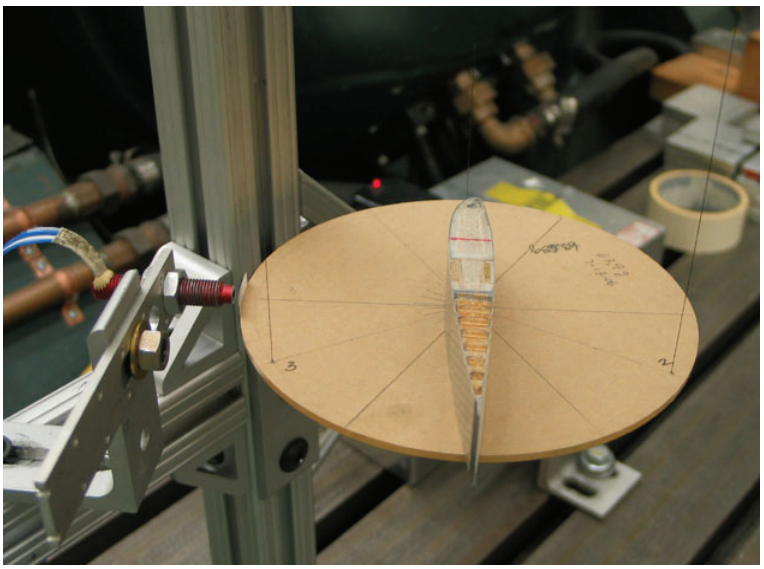

Figure 5. Measurement of the polar mass moment of inertia for a cut-out section using the trifilar pendulum.

TABLE 4. TIME PERIOD OF OSCILLATIONS MEASURED FOR H1B CUT SECTIONS

No. of Scans	Time Period, sec			
	Section A	Section C	Section D	Section F
1	0.718436	0.712524	0.502541	0.73254
2	0.719181	0.712324	0.502345	0.732435
3	0.719112	0.712413	0.502469	0.73253
4	0.718821	0.712195	0.502389	0.732582
5	0.718636	0.712533	0.502481	0.732452
6	0.718726	0.712146	0.502159	0.732679
7	0.718763	0.712191	0.502104	0.732534
8	0.718793	0.712063	0.502197	0.73246
9	0.718981	0.711984	0.502379	0.732387
10	0.718743	0.712082	0.501984	0.732499
11	0.718735	0.71205	0.501794	0.732381
12	0.718767	0.712218	0.501049	0.732295
13	0.718551	0.712115	0.501465	0.73238
14	0.718893	0.712226	0.50257	0.732237
15	0.718945	0.711916	0.502309	0.732193
16	0.718696	0.712135	0.502521	0.732358
17	0.718612	0.71191	0.50091	0.732311
18	0.71878	0.711974	0.500445	0.732394
19	0.718642	0.712116	0.501305	0.732439
20	0.718654	0.711971	0.502081	0.732327
21	0.718564	0.712094	0.501819	0.732278
22	0.718696	0.711716	0.501369	0.732307
23	0.718555	0.712128	0.500848	0.732384
24	0.71854	0.711951	0.502235	0.732168
25	0.718852	0.711876	0.501618	0.732365
26	0.718811	0.711900	0.500377	0.732361
27	0.718600	0.711799	0.500963	0.732363
28	0.718447	0.712151	0.500901	0.732261
29	0.718033	0.711635	0.501374	0.732319
30	0.719321	0.711901	0.501516	0.732197
31	0.7189791	0.7115144	0.5015562	0.7322398
32	0.7188179	0.7116963	0.5012538	0.7321769
33	0.7187343	0.7119638	0.5011115	0.7322537
34	0.7189463	0.7117866	0.5010785	0.732542
35	0.7187833	0.7120377	0.5013631	0.7319772
36	0.718413	0.7114913	0.5008766	0.732253
37	0.7187677	0.7116729	0.5018594	0.7322524
38	0.7187611	0.7118541	0.4994735	0.7322852
39	0.7185838	0.711904	0.4986774	0.7318549
40	0.7184031	0.712002	–	0.7322085

Elastic Axis

The elastic axis (EA) is defined as the chordwise position of the blade where the vertical bending introduces no tosional motion. Figure 6 shows the measurement setup for the determination of the EA. A clamped-free blade, having effective length of about 946 mm, with a 76.2-mm-wide steel root fixture with a loading fixture at the tip, is constructed for this purpose. The number 4 blade (H1R) is used for the test. The position of loading along the chord can be varied using a sliding table attached to the loading fixture, and the amount of loading is measured by an interface load-cell. To measure the angular displacements, both dial gauges and an auto-collimator are installed near the root and the tip of the cantilevered blade, respectively. Two dial guages separated by 91 mm along the blade chord are used to measure the rotational angle with the resolution of 11.5 arcsecond. A third dial gauge is set to measure the chordwise travel of the sliding table. Two optical mirrors are mounted on the blade leading edge near the blade tip, and they are aligned with the auto-collimator to measure the angular displacement as indicated in figure 6. Once the measurement setup is completed, the load is applied first at the quarter chord position, and the angle of twist is determined by reading the collimator angle as well as the dial gauges. The loads are applied up to 11.2 N, which corresponds to the limit of the collimator reading. Next, the chordwise position of loading is moved toward leading edge or trailing edge until the relative twist angle becomes nearly zero, which represents the EA position. The measured EA of the blade uniform section is positioned at 20.5 mm (0.169 *c*) from the leading edge. The measurement error is within 0.5 deg by the collimator limit.

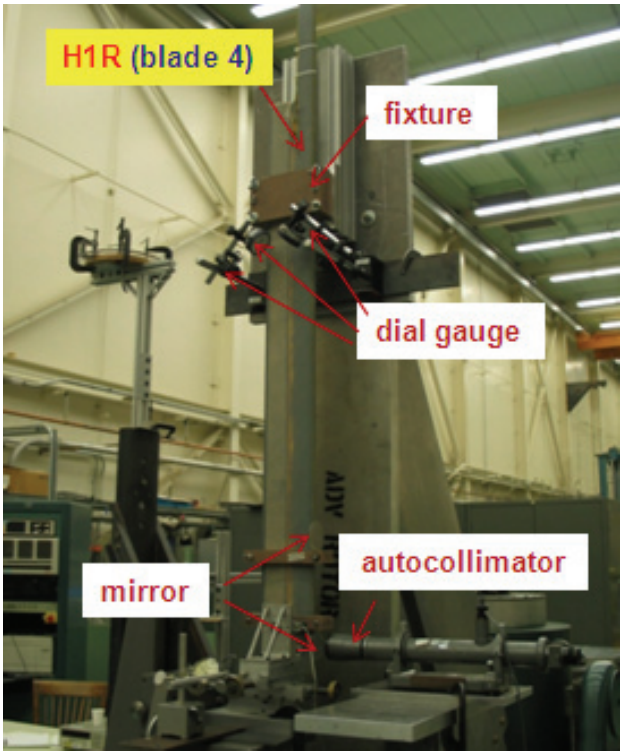

Figure 6. Measurement setup for the determination of elastic axis.

Section Stiffness

The stiffness measurements are made based on two techniques: the mirror method (ref. 11) and the 3-point bending technique (ref. 12). The first one uses a pair of mirrors attached on the blade surface while laser lights are beamed onto the mirrors. It is assumed that the section properties are uniform between the mirror pair. Figure 7 shows the schematic view of the mirror method for a fixed-free blade in bending. The laser lights are reflected from the mirrors onto the wall, separated at a distance D (see fig. 8). In the initial unloaded state, the laser beam is reflected at an angle 2θ and is positioned on the wall at a distance δ_0, as shown in figure 8. When the blade is under bending, the mirrors are rotated further to have an inclination angle 2β, and the laser reflection on the wall traverses to a distant location δ. The laser path angle β is determined using the geometric relationship shown in figure 7:

$$\beta = \frac{1}{2}\left(\tan^{-1} \frac{\delta + \delta_0}{D} - \theta \right) \tag{3}$$

By increasing the loads applied to the blade and the movement of laser reflections on the wall, the effective blade stiffness in bending is obtained between each mirror pair as:

$$EI = \frac{1}{2\beta / P}\left(a_1^2 - a_2^2\right) \tag{4}$$

where P is the applied force, and a_1 and a_2 denote the distances between the mirrors and the position of load (see fig. 7), respectively. In the actual measurements, the load is increasingly applied, and the slope of the laser reflection angle versus the applied load ($2\beta/P$) is obtained accordingly. A number of cycles are preceded using the same setup to ensure repeatability.

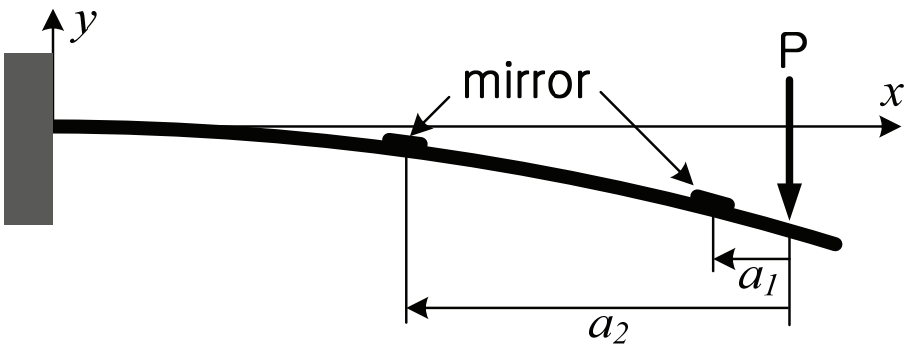

Figure 7. The mirror method for a blade in bending.

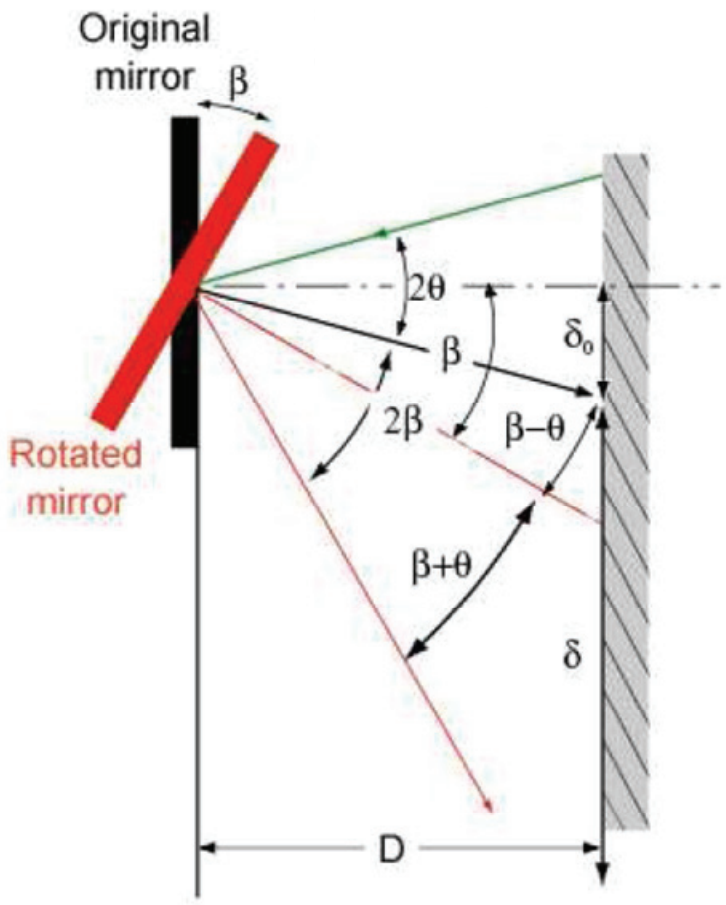

Figure 8. Geometry of the mirror method.

The torsion stiffness is obtained by measuring the angle of twist under a torque and is given by the relation:

$$GJ = \frac{l_1}{\phi / T} \tag{5}$$

where l_1 is the effective length of the blade between the end supports, ϕ is the angle of rotation, and T denotes the applied torque. The mirror method is again applied to determine the angle of twist between specified radial stations of the blade.

For the 3-point bending, the blade is placed on roller supports to simulate a simply supported boundary condition while the load is applied at the center (see fig. 9). Uniformity of blade properties between the end supports is assumed to obtain the blade elastic property. The bending stiffness is evaluated using the relation:

$$EI = \frac{l_2^3}{48 \cdot (\delta_c / P)} \tag{6}$$

where l_2 is the length between the end supports, δ_c denotes the deflection at the center, and δ_c / P represents the slope of the deflection-load curve. The deflection is measured using a pair of dial gauges having a resolution of 0.0001 inch each. The slope of the deflection-load curve is determined by averaging the measured records. This rather simple technique has proven efficient to determine the bending stiffness of the blade uniform section. In the following subsections, the measurement details of the flap bending, chord bending, and torsion stiffness are described.

Chord Bending

The 3-point bending method is used to determine the chord bending stiffness of the blade uniform section. Special fixtures and loading blocks were built for the boundary supports at the ends and at the application of the load, respectively. In addition, tilt platforms having ±2.86 deg adjustable range were placed underneath the end supports to accommodate the built-in twist angle of the HART I blade and to ensure that the loading axis remains perpendicular to the blade axis. Both lead bending (leading-edge down) and lag bending (trailing-edge down) tests were performed and then averaged for the chord bending stiffness. Figure 10 shows the measurement setup for the lag bending stiffness using the 3-point bending method. The length of the blade between the end supports, l_2, is 1.381 m, and the load (weight) P is increased from 5.528 kg up to 16.79 kg. The deflection is measured at the central station of the blade using a dial gauge having a resolution of 0.0001 inch (0.0254 mm). A total of 10 different measurements were made for either lead bending or lag bending. Tables 5 and 6 show the measurement records for the deflections at the center for lead bending and lag bending, respectively, with the increase of the weights. Figures 11 and 12 show the linear regressions of the load-deflection curves for 10 different measurements on lead bending and lag bending cases, respectively. The measured slopes indicate some scatter between the different cases. The standard deviation of the slopes in reference to the mean value is 2.16 percent for the lag bending and 2.51 percent for the lead bending. The slopes of each load-deflection curve in the dimension of N/m are shown in table 7. Inserting the averaged values of the load-deflection curves into Eq. (6), the lead bending or the lag bending stiffness can be obtained. The averaged values are 3,833 N-m^2 for the lead bending and 4,232 N-m^2 for the lag bending. The chord bending stiffness, which is determined by averaging the lead bending and the lag bending stiffness, is 4,032 N-m^2. The estimated chord bending stiffness by DEI is 4,706 N-m^2, 17 percent higher than the measured value.

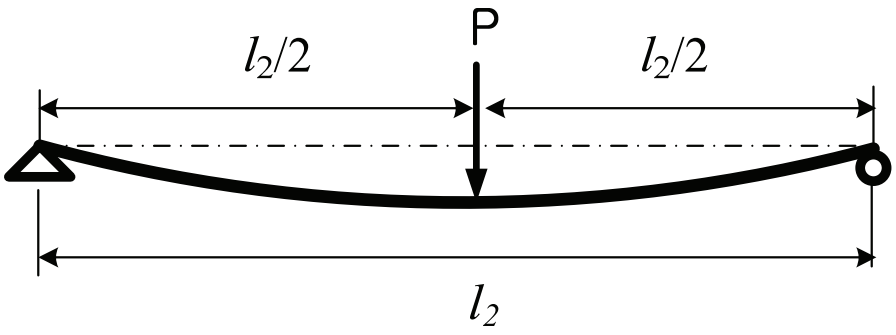

Figure 9. The simply supported blade in bending (3-point bending method).

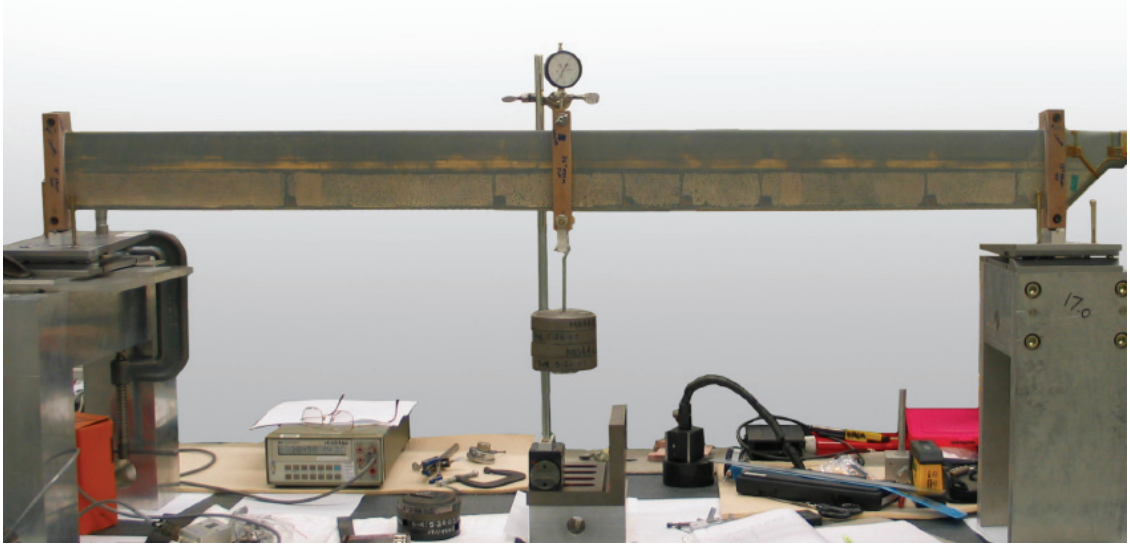

Figure 10. Measurement of the lag bending using a 3-point bending method.

TABLE 5. MEASURED DEFLECTIONS AT THE BLADE CENTRAL POSITION FOR THE LEAD BENDING

Load *P* kg	**Deflections at the Center δ_c, mm**									
0	0	0	0	0	0	0	0	0	0	0
5.528	0.742	0.712	0.730	0.687	0.687	0.707	0.681	0.694	0.687	0.697
9.528	1.371	1.269	1.318	1.239	1.267	1.262	1.234	1.247	1.242	1.244
12.25	1.790	1.693	1.721	1.658	1.678	1.670	1.635	1.645	1.635	1.647
14.97	2.201	2.102	2.140	2.000	2.074	2.076	2.028	2.036	2.033	2.036
16.79	2.480	2.371	2.406	2.312	2.350	2.330	2.294	2.294	2.292	2.297

TABLE 6. MEASURED DEFLECTIONS AT THE BLADE CENTRAL POSITION FOR THE LAG BENDING

Load *P* kg	**Deflections at the Center δ_c, mm**									
0	0	0	0	0	0	0	0	0	0	0
5.528	0.669	0.633	0.636	0.656	0.666	0.692	0.679	0.681	0.687	0.676
9.528	1.239	1.234	1.188	1.191	1.191	1.196	1.178	1.183	1.191	1.183
12.25	1.599	1.586	1.551	1.536	1.551	1.541	1.518	1.515	1.515	1.513
14.97	1.959	1.936	1.893	1.888	1.891	1.909	1.858	1.860	1.860	1.860
16.79	2.203	2.172	2.124	2.124	2.119	2.137	2.094	2.086	2.117	2.094

TABLE 7. SLOPES OF THE LOAD-DEFLECTION CURVE FOR THE LEAD-LAG BENDING

Case	Slopes of P/δ_c Curve, N/m									
Lead	65809	68926	67946	71194	69440	70065	71242	71261	71299	71222
Lag	74101	74625	76572	77075	77177	76942	78699	78889	78271	78663

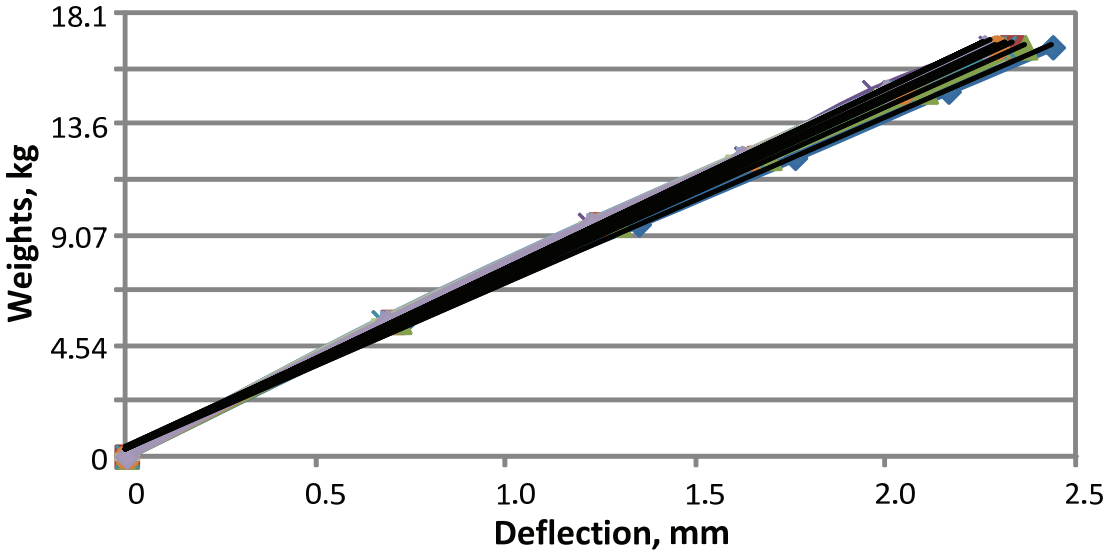

Figure 11. Linear regression of the load-deflection curve for the lead bending (data from table 5).

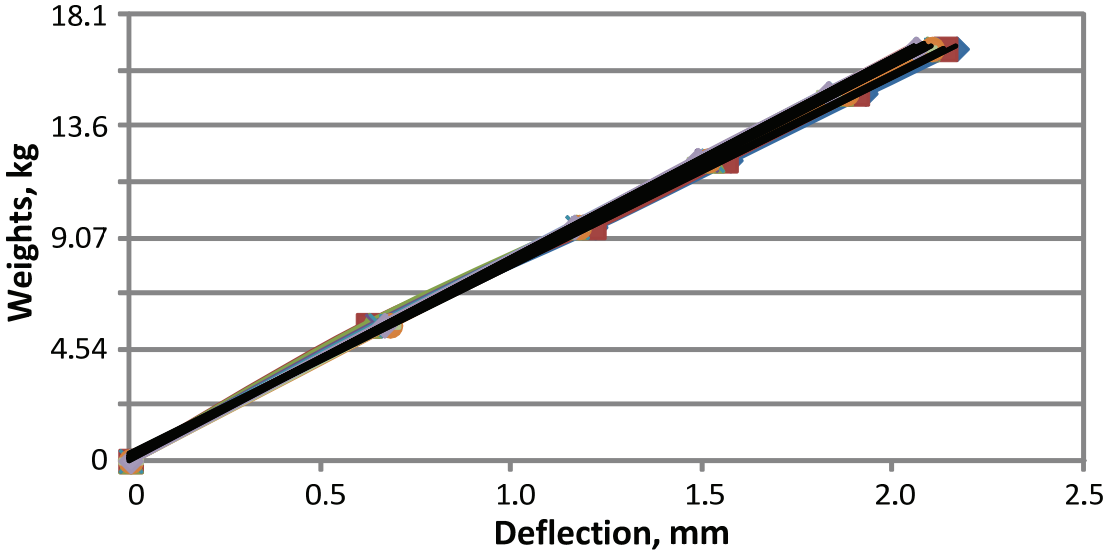

Figure 12. Linear regression of the load-deflection curve for the lag bending (data from table 6).

Flap Bending

The flap bending of the blade uniform section is obtained using the 3-point bending technique while the mirror method is used for the root section. Figure 13 shows the measurement setup for the 3-point bending to determine the flap bending stiffness of the HART I blade. The full span of the H1S blade is used for this property. The length between the supports at end is 1.214 m, and the weights applied at the center are increased up to 2.34 kg. At the maximum loading, the deflections at the center reach around 4.6 mm. The deflections are measured using a dial gauge installed at the center of the blade (see table 8). Figure 14 shows the linear regression of the load-deflection curves for 10 different measurements. As can be seen in the plot, the linearity is a good approximation for the elastic behavior of the blade. Most of the measured deflections form nearly identical curves with a few exceptions. Table 9 presents the slopes of the load-deflection curve P/δ_c for the 10 different measurements. The standard deviation of the data is about 1.2 percent in reference to the mean value of the load-deflection curve. Overall, the flap bending tests demonstrate reasonably good repeatability as compared with the chord bending tests. The flap bending stiffness is obtained by inserting the load-deflection curve P/δ_c into Eq. (6), which gives about 188.4 N-m^2 for the uniform section of the H1S blade. Similar tests were also performed for the cut-down section of H1B (blade 3), as shown in figure 15. In this case, the length between the end supports is 0.902 m. The measured flap bending obtained using the load-deflection curves is 182.9 N-m^2. The final value for the measured flap bending of the uniform portion of the HART I blade is obtained by averaging the values between the H1S and H1B cut-down sections, which result in 185.6 N-m^2.

The flap bending for the root portion of the HART I blade is determined using the mirror method. Figure 16 shows the actual measurement scene for the flap bending via the mirror method. The blade (H1S) is clamped at the root using the L-bracket made of stainless steel and hung vertically. The load is applied near the tip in the flap-up direction using a pulley connected with a series of weights. The load remains perpendicular to the blade chord at the tip. A total of six mirrors are attached on the blade surface: four of them are for the blade root and two are for the uniform blade. The mirrors from the top to the lower end of the root region are placed at 1.796 m, 1.758 m, 1.692 m, 1.662 m, and 1.557 m, measured from the blade tip, respectively. It is noted that the bracket itself is used as a top mirror. The direct distance between the mirror and the laser on the wall is about 7.3 m. The vertical distances (δ_0) from the ideally leveled laser to the undeflected laser for the mirrors are –1.39 m, 0.19 m, –0.69 m, 0.11 m, and –0.205 m, respectively. The load is increased from 0.199 kg to 1.69 kg. Table 10 shows the measured records for the traverse distance of laser reflections on the wall for each mirror. The mirrors are designated M1 to M5 located from the top. At each mirror pair, the delta slope ($2\beta/P$) is evaluated by measuring the traverse distance of the laser reflections on the wall, and these are inserted in Eq. (4) for the flap bending stiffness between the mirror pair. The measurement is conducted for both H1R (blade 4) and H1S (spare). The flap bending stiffness between each mirror pair is averaged for H1R and H1S, and the results are presented in table 11.

Torsion Stiffness

The blade torsion stiffness is obtained using Eq. (5). The mirror method is again introduced to determine the ratio of the twist angle to the torque (ϕ/T). Figure 17 shows the setup for the measurement of the torsion stiffness. Three mirrors are attached on the blade surface at 0.782 m, 0.4 m, and 0.0534 m, relative to the blade tip. The mirrors are designated M1, M2, and M3,

respectively. The nose-down torque up to 15.8 N-m is applied at the EA location. The amount of torque is measured by a torque cell with an excitation voltage of 5.014 V and a conversion factor of 2733.2 N-m/V. The distance between the mirror and the wall is approximately 4.76 m. The vertical distances from the laser sources to the reflections are 0.422 m, 0.273 m, and 0.603 m, respectively. Table 12 shows the measurement records for the traverse distance of laser reflections marked on the wall for each mirror. The measurements are made for the H1R blade (blade 4) with either pitch-up or pitch-down position, and they are averaged for about six different measurements. The final measured torsion stiffness is determined to be 128.5 N-m^2 for the uniform section.

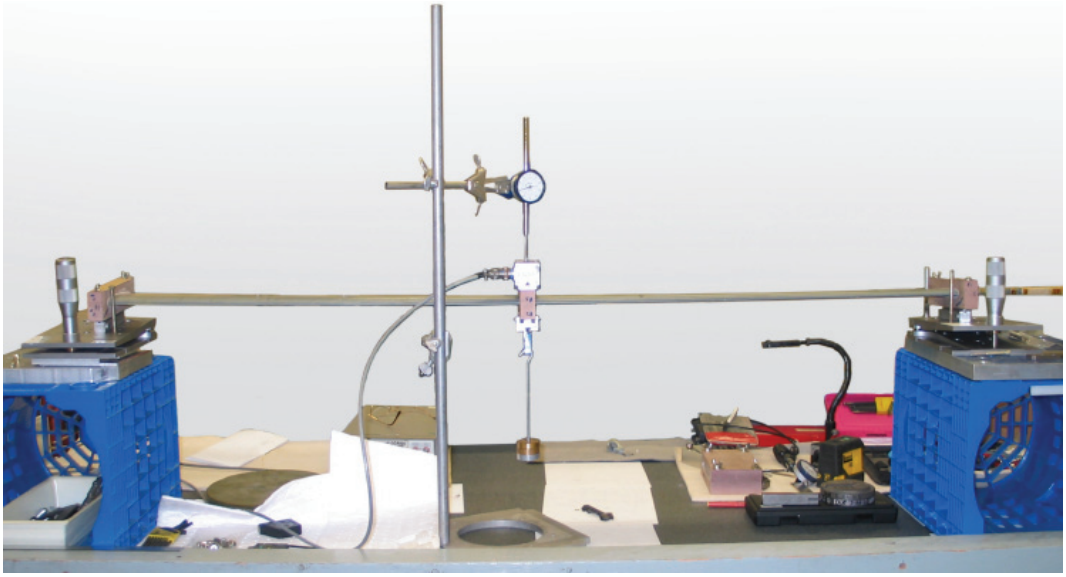

Figure 13. Measurement of the flap bending for H1S blade using a 3-point bending method.

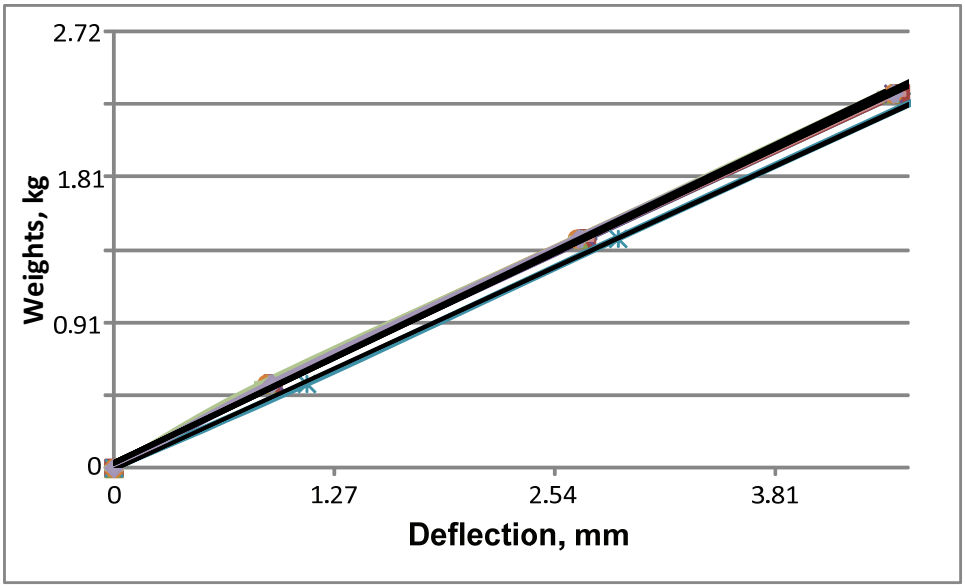

Figure 14. Linear regression of the load-deflection curve for the flap bending (data from table 8).

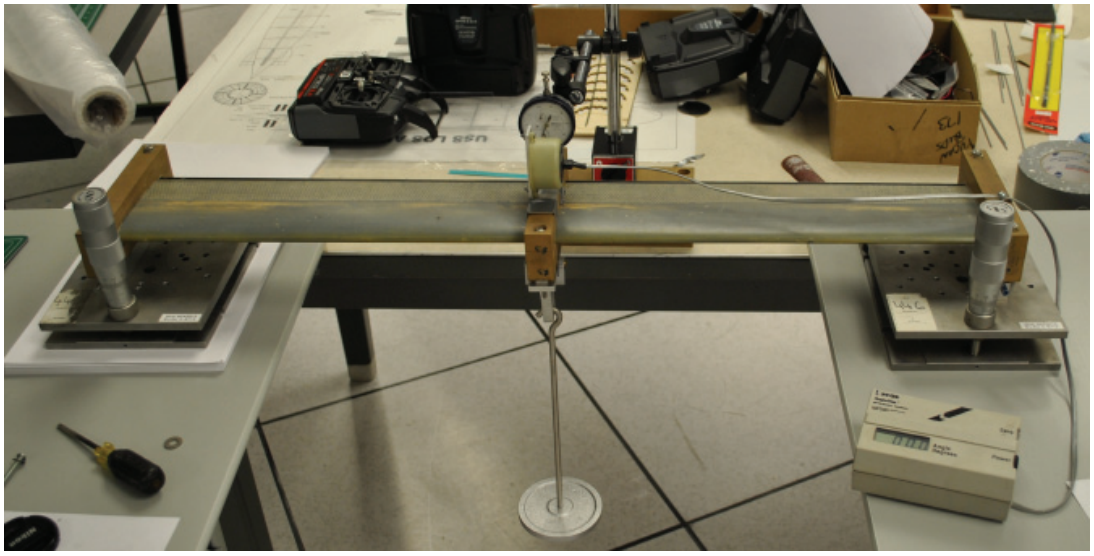

Figure 15. Measurement of the flap bending for H1B cut section using a 3-point bending method.

Figure 16. Measurement of the flap bending with the mirror method.

Figure 17. Measurement of the torsion stiffness with the mirror method.

TABLE 8. MEASURED DEFLECTIONS AT THE BLADE CENTRAL POSITION FOR THE FLAP BENDING

Load *P* kg	**Deflections at the Center δ_c, mm**									
0	0	0	0	0	0	0	0	0	0	0
1.161	0.0359	0.036	0.0344	0.0369	0.0437	0.0346	0.0352	0.0355	0.0339	0.0358
3.161	0.1073	0.107	0.1051	0.1073	0.1142	0.1049	0.106	0.1066	0.1051	0.1053
5.161	0.1782	0.1781	0.1759	0.1765	0.1856	0.1764	0.1774	0.1772	0.1749	0.1766

TABLE 9. SLOPES OF THE LOAD-DEFLECTION CURVE FOR THE FLAP BENDING

Case	**Slopes of P/δ_c Curve, N/m**									
Flap	5035.0	5041.0	5093.2	5093.0	4886.2	5083.6	5056.6	5061.7	5113.9	5090.7

TABLE 10. THE TRAVERSE DISTANCE OF LASER DOTS ON THE WALL FOR EACH MIRROR (FLAP BENDING)

Load, kg	Traverse Distance of Laser, mm				
	M1	**M2**	**M3**	**M4**	**M5**
0	0	0	0	0	0
0.199	1.5	4	10	15.5	36
0.398	3	8	21	31.5	72
0.597	5.5	13	32	47.5	108.5
0.795	7.5	18	43	64	145.5
0.994	10	22	54	80	183
1.193	12	27.5	65	96	220
1.392	14.5	32	76	112	257
1.591	17	37	87	128.5	294
1.690	N/A	39.5	92.5	136.5	312

TABLE 11. MEASURED FLAP BENDING FOR BLADE ROOT REGION

Station	Flap Bending Stiffness, N-m^2
1.796 m – 1.758 m	656.1
1.758 m – 1.692 m	528.3
1. 692 m – 1.662 m	270.1
1.662 m – 1.557 m	219.4

TABLE 12. THE TRAVERSE DISTANCE OF LASER DOTS ON THE WALL FOR EACH MIRROR (TORSION STIFFNESS)

Load, kg	Traverse Distance of Laser, mm		
	M1	**M2**	**M3**
2.26	0	100	100
4.54	38.5	203	267
6.79	76	304.5	433.4
9.06	115.5	408.5	605
11.31	155	516	784
13.56	196.5	631	977.5
14.69	217	687	1074

TABLE 13. COMPARISON OF BLADE STRUCTURAL PROPERTIES OF HART I UNIFORM SECTION

Property	Measured	DEI	% Difference
Flap bending	190.1 N-m^2	185.6 N-m^2	2.37%
Chord bending	4706 N-m^2	4032 N-m^2	14.3%
Torsion stiffness	134 N-m^2	128.5 N-m^2	4.10%
Center of gravity	0.245 *c*	0.265 *c*	8.16%
Elastic axis	0.20 *c*	0.169 *c*	15.5%
Polar MOI at CG	0.000623 kg-m	0.000569 kg-m	8.67%

Comparison With Estimated DEI Values

The present measured structural property data obtained for the uniform portion of the HART I blade are compared against the estimated values obtained by DEI, the manufacturer of HART I blades. Table 13 shows the comparison results. A significant change is seen in the blade structural properties. Generally, the measured data indicate more flexible blade stiffness compared to the DEI values. The maximum difference is about 14.3 percent for the chord bending stiffness. DEI predictions indicate that the chordwise CG is located very close to the QC axis and shifted in the direction of the leading edge. On the contrary, the measured CG indicates a shifting to the trailing edge. In addition, the measured EA is positioned far to the leading edge compared to the DEI predictions. Overall, the measured offset between CG and EA is larger by about 5 percent chord length than the estimated value by DEI. These differences in measured blade properties (i.e., softening of blade stiffness combined with increased offsets) are expected to introduce larger couplings between aerodynamics and structures of HART I blades than DEI values, which will make the rotor aeroelastic analysis more complex.

Almost all of the blade properties are measured for the blade uniform portion. Only the flap bending is considered for the measurement of the blade root section. The lack of data in this region of blade is overcome by introducing the DEI values and combining them with the present measured property data results in the complete set of HART I structural properties. Figures 18 through 25 show the comparison between the present measured data and the DEI values. The blade properties are presented as a function of the blade span coordinates. It is observed that the DEI values generally overestimate the blade section stiffness by up to 30 percent in the flap bending of the blade root section.

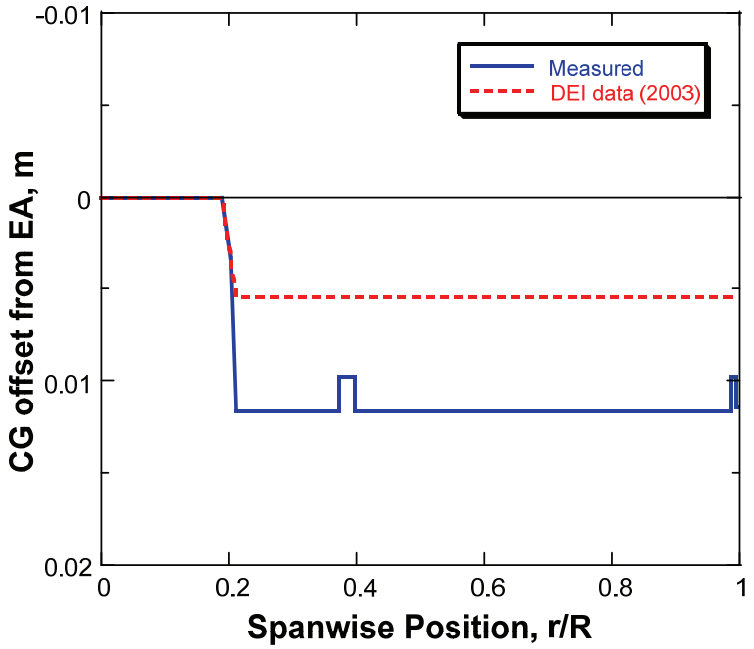

Figure 18. Comparison of the center of gravity offset from the elastic axis.

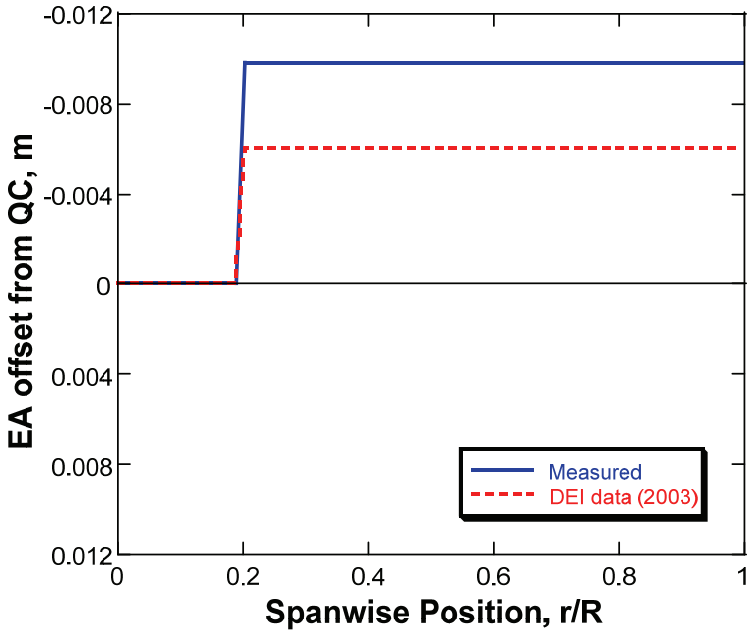

Figure 19. Comparison of the elastic axis offset from the quarter chord axis.

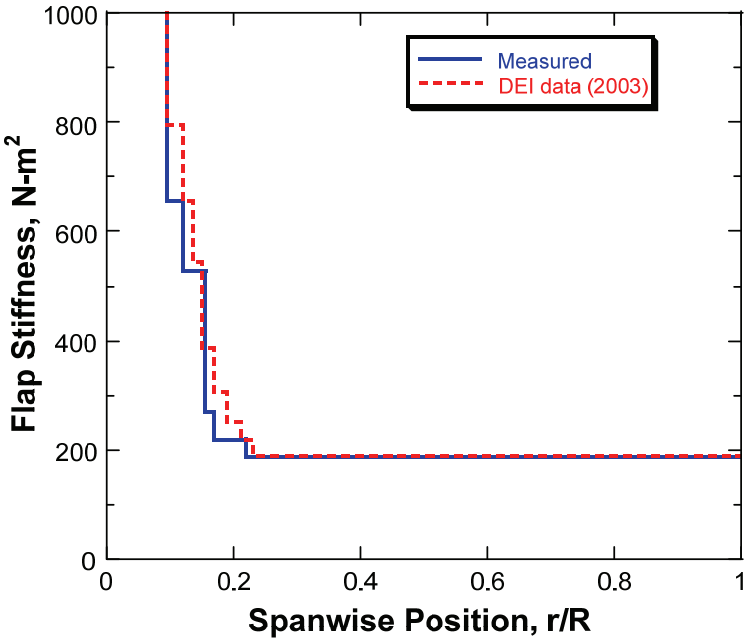

Figure 20. Comparison of flap bending stiffness along the blade length.

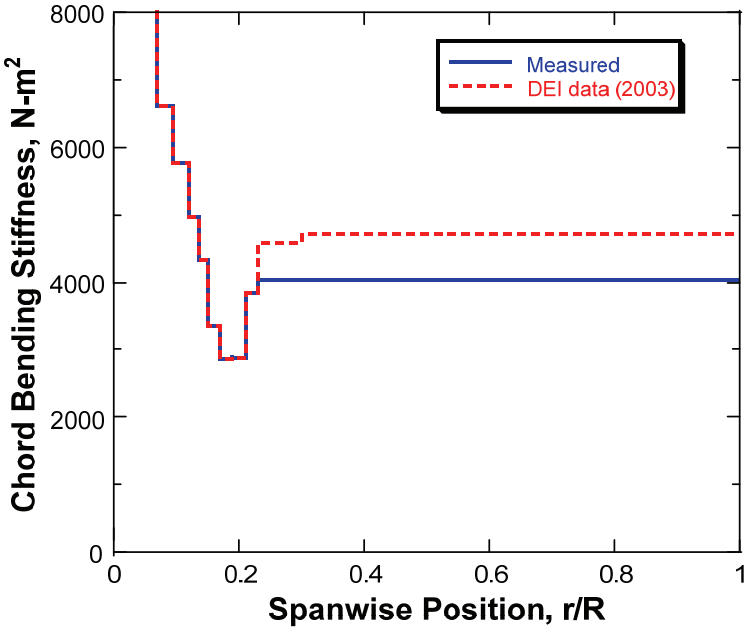

Figure 21. Comparison of chordwise bending stiffness along the blade length.

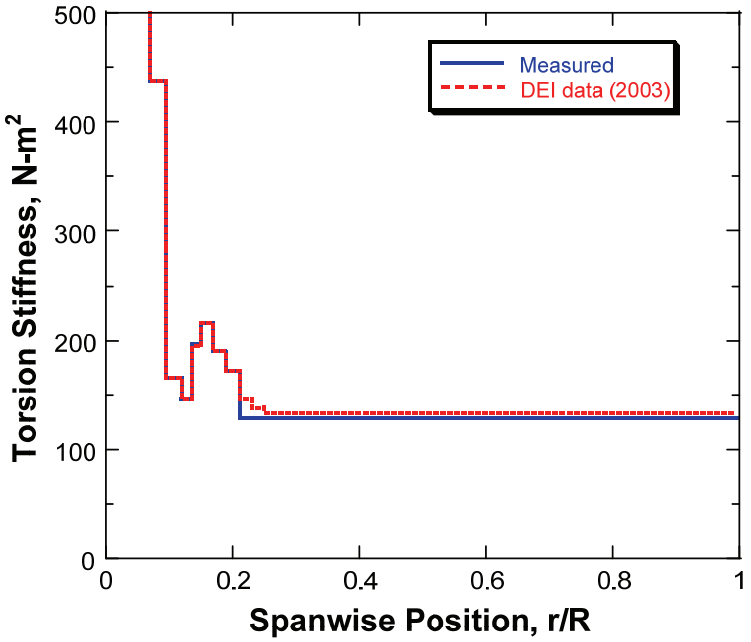

(c) Torsion

Figure 22. Comparison of torsion stiffness along the blade length.

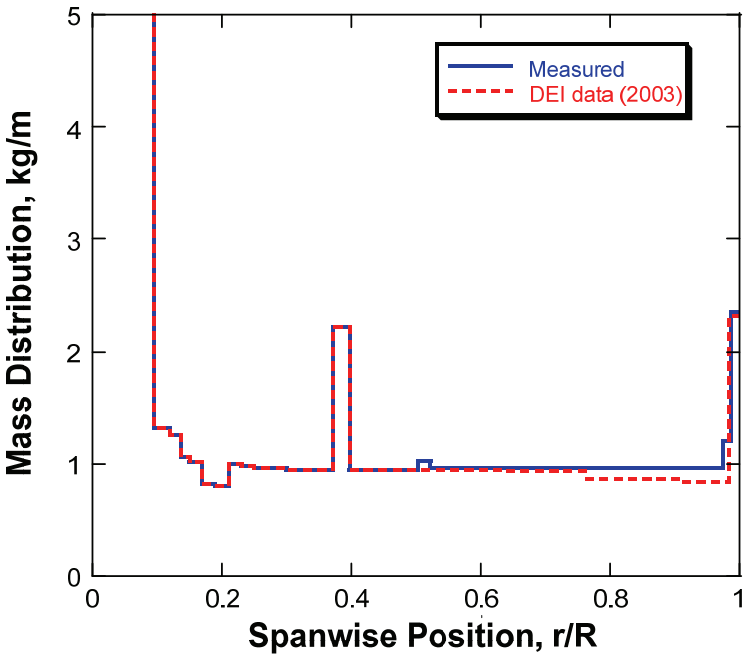

Figure 23. Comparison of mass distribution along the blade length.

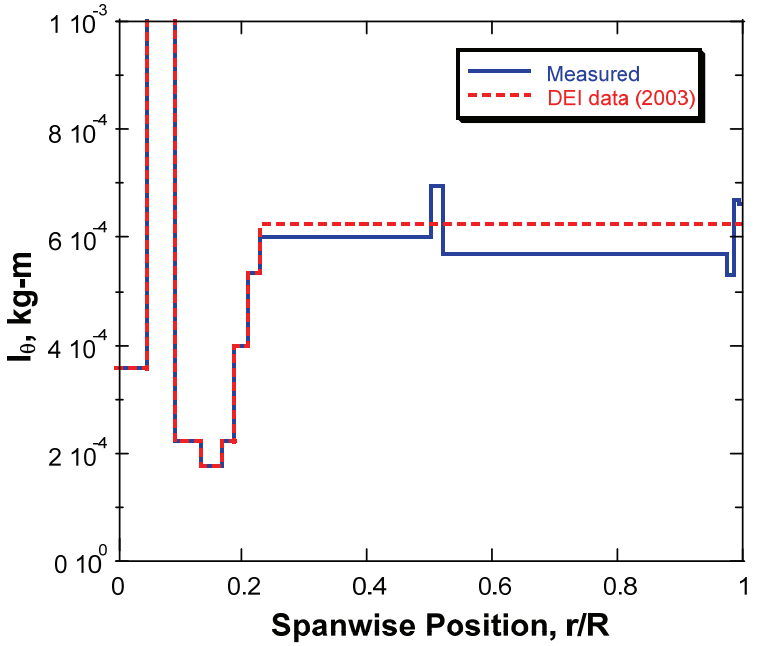

Figure 24. Comparison of polar mass moment of inertia along the blade length.

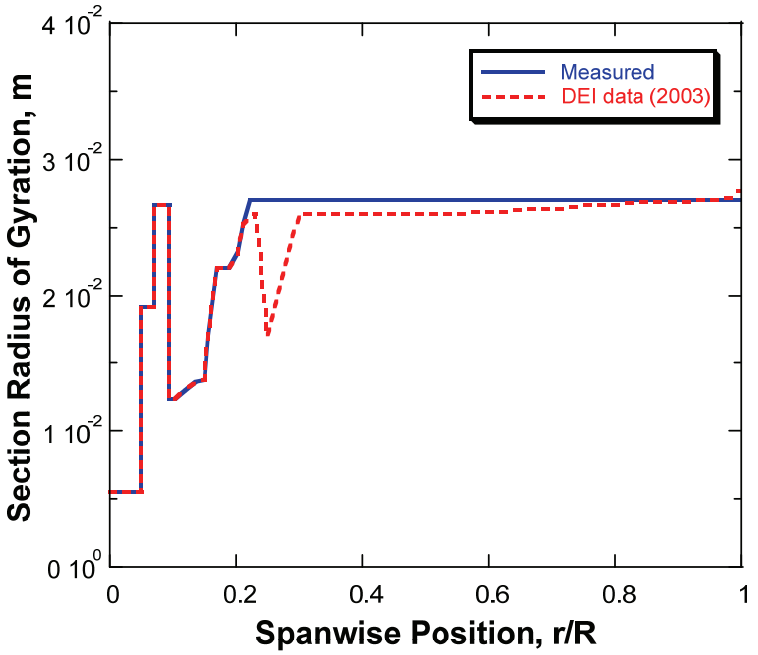

Figure 25. Comparison of section radius of gyration along the blade length.

Expanded Blade Property Data

The complete set of structural property data for the HART I blade in Comprehensive Analytical Model of Rotorcraft Aerodynamics and Dynamics II (CAMRAD II) input format (ref. 13) is summarized in table 14. The first column (r/R) denotes the blade coordinates nondimensionalized by the blade radius (R = 2 m). Y_{EA} and Z_{EA} denote the location of the EA parallel and perpendicular to the chord line of the blade from the QC axis, respectively. The sign convention for Y and Z axes is defined as positive when moved toward the trailing edge and the vertical direction, respectively. The next two columns describe the position of CG from the EA in the Y and Z coordinates. It is remarked that the position of tension center is not measured and assumed to coincide with the EA location. Twist and Mass, appearing after the CG offsets, denote the blade pretwist angle and the mass distribution, respectively. The blade flap bending, EI_{FLAP}, chord bending, EI_{CHD}, and torsion stiffness, GJ, follow next. The next column is the cross-sectional radius of gyration in polar coordinates, Kp polar radius of gyration. The final two columns represent the polar moment of inertia at CG for I_θ and I_P, respectively. All the values presented in table 14 are given in the International System of Units (SI).

COMPARISON OF ROTOR NATURAL FREQUENCIES

In figure 26, predicted natural frequencies of the HART I rotor using the measured properties are compared against the test data (ref. 11), as well as those obtained using DEI property data. The predicted results are obtained in vacuum condition using CAMRAD II (ref. 13). The frequency values are nondimensionalized by the rotor nominal speed (Ω_0 = 1040 RPM). It should be noted that the measured frequencies are obtained for the instrumented blade (blade 1) and only available at nonrotating condition. For the control system modeling, a linear pitch link model with the spring constant of 0.43 million N/m is adopted, which is equivalent to a pitch bearing stiffness of 1706 N-m/rad, to match the first torsion frequency of the instrumented blade. In general, the DEI data result in higher bending and torsion frequencies than the measured values. It is observed that the present predictions indicate reasonable agreements for lead-lag bending and torsion frequencies but show slightly higher frequencies in flap bending compared to the measured data. The main reason is because the measured frequencies are taken from the instrumented blade while the present structural properties are obtained from the rest of the blades (i.e., uninstrumented blades). Considering the fact that the instrumented blade is heavier than the other blades by about 6 percent (ref. 11), the present frequencies appear to have a reasonable correlation with the test data.

Further investigation was made in Jung et al. (ref. 14) for the correlation of airloads and structural loads of the HART I rotor in descending flight condition, with and without higher harmonic pitch control inputs, using the measured blade properties. It was observed that, in general, more improved predictions were achieved with the measured data.

TABLE 14. SUMMARY OF HART I BLADE PROPERTIES

r/R	Y_{EA}, m	Z_{EA}, m	Y_{CG}, m	Z_{CG}, m	Twist deg	Mass kg/m	EI_{FLAP} N-m^2	EI_{CHD} N-m^2	GJ N-m^2	k_P, m	I_{θ_CG} kg-m	I_{P_CG} kg-m
0	0	0	0	0.0001	3.84	10.706	25482.82	25482.82	10000.65	0.0056	0.000356	0.000311
0.025	0	0	0	0.0001	3.84	10.706	25482.82	25482.82	10000.65	0.0056	0.000356	0.000311
0.0251	0	0	0	0.0001	3.84	10.529	41237.32	41237.32	10000.65	0.0056	0.000356	0.000311
0.05	0	0	0	0.0001	3.84	10.529	41237.32	41237.32	10000.65	0.0056	0.000356	0.000311
0.0501	0	0	0	0.0001	3.84	9.633	39486.87	61984.91	10000.65	0.0192	0.003559	0.003514
0.0699	0	0	0	0.0001	3.84	9.633	39486.87	61984.91	10000.65	0.0192	0.003559	0.003514
0.07	0	0	0	0.0001	3.84	10.706	1004.57	6600.15	438.03	0.0266	0.007562	0.007517
0.095	0	0	0	0.0001	3.84	10.706	1004.57	6600.15	438.03	0.0266	0.007562	0.007517
0.0951	0	0	0	0.0001	3.84	1.321	656.1	5767.9	166.45	0.0124	0.000222	0.000178
0.12	0	0	0	0	3.84	1.321	656.1	5767.9	166.45	0.013	0.000222	0.000178
0.1201	0	0	0	0	3.84	1.25	528.3	4961.69	146.37	0.013	0.000222	0.000178
0.135	0	0	0	-0.00002	3.84	1.25	528.3	4961.69	146.37	0.0136	0.000222	0.000178
0.1351	0	0	0	-0.00002	3.84	1.068	528.3	4318.7	195.42	0.0136	0.000178	0.000133
0.15	0	0	0	-0.00002	3.84	1.068	528.3	4318.7	195.42	0.0138	0.000178	0.000133
0.1501	0	0	0	-0.00002	3.84	1.02	528.3	3340.16	214.92	0.0138	0.000178	0.000133
0.155	0	0	0	0.00002	3.84	1.02	528.3	3340.16	214.92	0.017	0.000178	0.000133
0.1551	0	0	0	0.00002	3.84	1.02	270.1	3340.16	214.92	0.017	0.000178	0.000133
0.17	0	0	0	0.00002	3.84	1.02	270.1	3340.16	214.92	0.022	0.000178	0.000133
0.1701	0	0	0	0.00002	3.84	0.828	219.4	2849.65	189.96	0.022	0.000222	0.000178
0.19	0	0	0	0	3.84	0.828	219.4	2849.65	189.96	0.022	0.000222	0.000178
0.1901	0	0	0	0	3.84	0.8	219.4	2875.27	172.48	0.022	0.0004	0.000356
0.20225	-0.00606	0.00118	0.003322	-0.0007	3.84	0.8	219.4	2875.27	172.48	0.0232	0.0004	0.000356
0.20226	-0.00606	0.00118	0.003322	-0.0007	3.84	0.8	219.4	2875.27	172.48	0.0232	0.0004	0.000356

TABLE 14. SUMMARY OF HART I BLADE PROPERTIES (CONTINUED)

r/R	X_{EA}, m	Z_{EA}, m	X_{CG}, m	Z_{CG}, m	Twist deg	Mass kg/m	EI_{FLAP} N-m^2	EI_{CHD} N-m^2	GJ N-m^2	k_P, m	I_{θ_CG} kg-m	I_{P_CG} kg-m
0.21	-0.0098	0.00118	0.01161	-0.00114	3.84	0.8	219.4	2875.27	172.48	0.0252	0.0004	0.000356
0.2101	-0.0098	0.00118	0.01161	-0.00114	3.84	0.996	219.4	3825.3	128.5	0.0252	0.000534	0.000489
0.22	-0.0098	0.00118	0.01161	-0.00022	3.84	0.996	219.4	3825.3	128.5	0.027	0.000534	0.000489
0.2201	-0.0098	0.00118	0.01161	-0.00022	3.8392	0.996	185.6	3825.3	128.5	0.027	0.000534	0.000489
0.23	-0.0098	0.00118	0.01161	-0.00022	3.76	0.996	185.6	3825.3	128.5	0.027	0.000534	0.000489
0.2301	-0.0098	0.00118	0.01161	-0.00022	3.7592	0.982	185.6	4032	128.5	0.027	0.0006	0.000556
0.25	-0.0098	0.00118	0.01161	-0.00022	3.6	0.982	185.6	4032	128.5	0.027	0.0006	0.000556
0.2501	-0.0098	0.00118	0.01161	-0.00022	3.5992	0.958	185.6	4032	128.5	0.027	0.0006	0.000556
0.3	-0.0098	0.00118	0.01161	-0.00022	3.2	0.958	185.6	4032	128.5	0.027	0.0006	0.000556
0.3001	-0.0098	0.00118	0.01161	-0.00022	3.1992	0.948	185.6	4032	128.5	0.027	0.0006	0.000556
0.3714	-0.0098	0.00118	0.01161	-0.00022	2.6288	0.948	185.6	4032	128.5	0.027	0.0006	0.000556
0.3715	-0.0098	0.00118	0.0098	-0.00022	2.628	2.212	185.6	4032	128.5	0.027	0.000603	0.00056
0.397	-0.0098	0.00118	0.0098	-0.00022	2.424	2.212	185.6	4032	128.5	0.027	0.000603	0.00056
0.3971	-0.0098	0.00118	0.01161	-0.00022	2.4232	0.948	185.6	4032	128.5	0.027	0.0006	0.000556
0.503	-0.0098	0.00118	0.01161	-0.00022	1.576	0.948	185.6	4032	128.5	0.027	0.0006	0.000556
0.5031	-0.0098	0.00118	0.01161	-0.00022	1.5752	1.027	185.6	4032	128.5	0.027	0.000694	0.000643
0.522	-0.0098	0.00118	0.01161	-0.00022	1.424	1.027	185.6	4032	128.5	0.027	0.000694	0.000643
0.5221	-0.0098	0.00118	0.01161	-0.00022	1.4232	0.958	185.6	4032	128.5	0.027	0.000569	0.000528
0.974	-0.0098	0.00118	0.01161	-0.00022	-2.192	0.958	185.6	4032	128.5	0.027	0.000569	0.000528
0.9741	-0.0098	0.00118	0.01161	-0.00022	-2.1928	1.2	185.6	4032	128.5	0.027	0.00053	0.000492
0.987	-0.0098	0.00118	0.01161	-0.00022	-2.296	1.2	185.6	4032	128.5	0.027	0.00053	0.000492
0.9871	-0.0098	0.00118	0.0098	-0.00022	-2.2968	2.342	185.6	4032	128.5	0.027	0.00067	0.000622
0.994	-0.0098	0.00118	0.0098	-0.00022	-2.352	2.342	185.6	4032	128.5	0.027	0.00067	0.000622
0.9941	-0.0098	0.00118	0.0114	-0.00022	-2.3528	2.342	185.6	4032	128.5	0.027	0.000664	0.000616
1	-0.0098	0.00118	0.0114	-0.00022	-2.4	2.342	185.6	4032	128.5	0.027	0.000664	0.000616

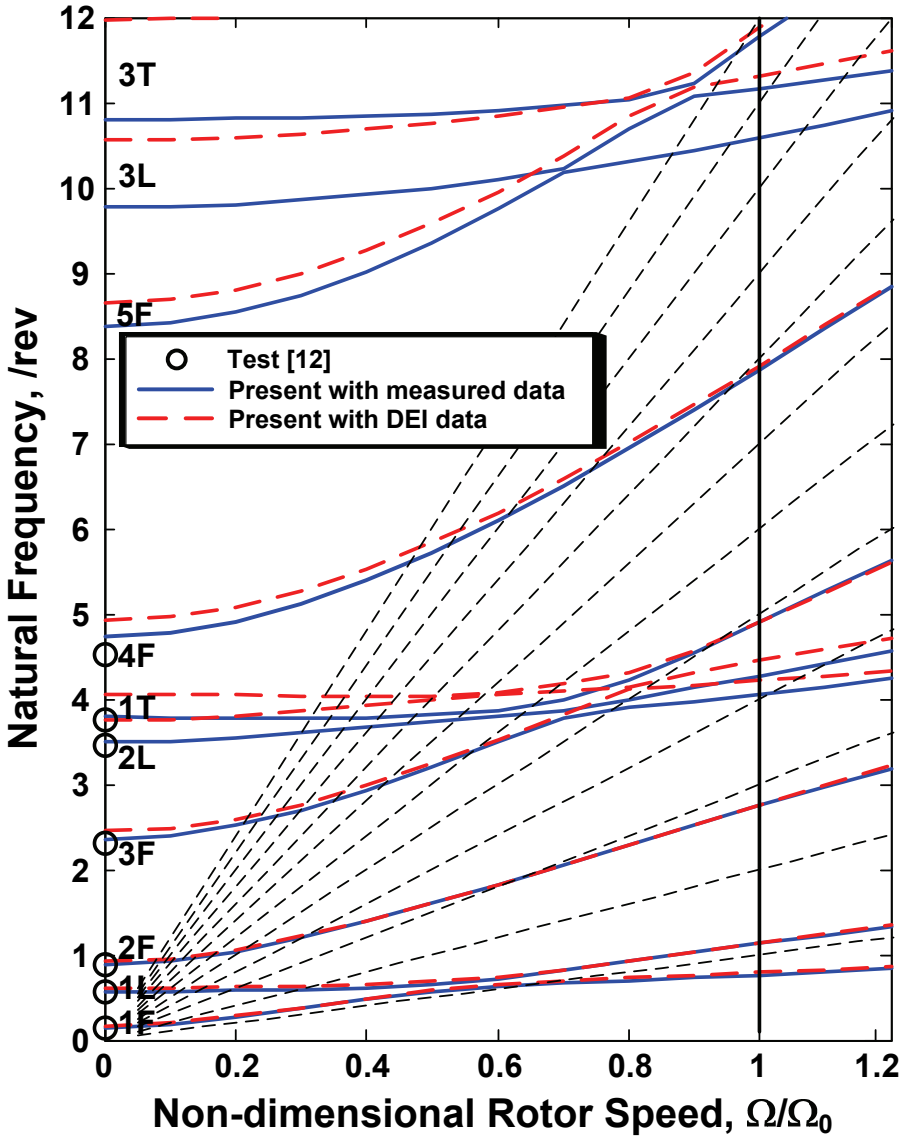

Figure 26. Comparison of rotor natural frequencies.

CONCLUSIONS

The elastic properties of HART I blades were measured using well-established test techniques. The following conclusions were drawn from this study.

1) The blade properties were measured using several test techniques. Both flap and chordwise bending stiffness in the blade uniform sections were measured using the 3-point bending method, while the flap bending in the inboard root section and the torsion stiffness in the blade uniform section were measured using the mirror method. The inertia properties were measured using the trifilar pendulum technique.

2) The measured blade properties were compared to the estimated values provided by DEI, the company that designed and built the HART I blades. It was found that the deviation was up to 30 percent for the flap bending over the blade root sections and 14.3 percent for the chord bending over the blade uniform section. As compared with the DEI estimations, the measured elastic axis (EA) was located more toward the leading edge and the center of gravity (CG) was shifted aft toward the trailing edge, resulting in larger offsets between CG and EA.

3) The comparison of rotor natural frequencies indicated that the present predictions with measured blade properties were in reasonable agreement with the test data, as compared with the predictions using DEI data.

REFERENCES

1. Yu, Y. H.; Gmelin, B.; Heller, H.; Philippe, J. J.; Mercker, E.; and Preisser, J. S.: HHC Aeroacoustics Rotor Test at the DNW—The Joint German/French/US HART Project. 20th European Rotorcraft Forum, Amsterdam, Netherlands, 1994.
2. Johnson, W.: Milestones in Rotorcraft Aeromechanics. NASA TP-2011-215971, 2011.
3. Tung, C.; Gallman, J. M.; Kube, R.; Wagner, W.; van der Wall, B.; Brooks, T. F.; Burley, C. L.; Boyd, Jr., D. D.; Rahier, G.; and Beaumier, P.: Prediction and Measurement of Blade-Vortex Interaction Loading. CEAS/AIAA Aeroacoustics Conference, Munich, Germany, June 12–15, 1995.
4. Lim, J. W.; Yu, Y. H.; and Johnson, W.: Calculation of Rotor Blade-Vortex Interaction Airloads Using a Multiple-Trailer Free-Wake Model. J. of Aircraft, vol. 40, no. 6, Nov.–Dec. 2003, pp. 1123–130.
5. Yeo, H., and Johnson, W.: Assessment of Comprehensive Analysis Calculation of Airloads on Helicopter Rotors. J. of Aircraft, vol. 42, no. 5, 2005, pp. 1218–1228.
6. Yeo, H., and Johnson, W.: Prediction of Rotor Structural Loads With Comprehensive Analysis. J. of the American Helicopter Society, vol. 53, no. 2, 2008, pp. 193-209.
7. Shekoski, T., and Tram L. H.: Blade Qualification and Accepatance Data Report, and Instrumentation and Calibration Report. ATI Document no. 167, Advanced Technologies, Inc., July 1996.
8. Ogorkiewicz, R. M., and Mucc, P. E. R.: Testing of Fibre-Plastics Composites in Three-Point Bending. Composites, vol. 2, no. 3, 1971, pp. 139–145.
9. Hughes, G. W.: The Trifilar Pendulum and Its Application to the Experimental Determination of Moments of Inertia. ASME Paper 57-SA-51, 1957.
10. Sharpe, D. L.: An Experimental Investigation of the Flap-Lag-Torsion Aeroelastic Stability of a Small-Scale Hingeless Helicopter Rotor in Hover. NASA TP-2546 (AVSCOM TR 85-A-9), Jan. 1986.

11. Splettstoesser, W. R.; Kube, R.; Seelhorst, U.; Wagner, W.; Boutier, A.; Micheli, F.; Mercker, E.; and Pengel, K.: Higher Harmonic Control Aeroacoustic Rotor Test (HART)–Test Documentation and Representative Results. Institute Report IB 129-95/28, German Aerospace Center (DLR), Braunschweig, Germany, Dec. 1995.
12. Gere, J. M., and Timoshenko, S. P.: Mechanics of Materials. 6th ed., BCT Learning, Belmont, 2004.
13. Johnson, W.: CAMRAD II: Comprehensive Analytical Model of Rotorcraft Aerodynamics and Dynamics. Johnson Aeronautics, Palo Alto, CA, 1992.
14. Jung, S. N.; You, Y. H.; Lau, B. H.; Johnson, W.; and Lim, J. W.: Evaluation of Rotor Structural and Aerodynamic Loads Using Measured Blade Properties. 38th European Rotorcraft Forum, Amsterdam, Netherlands, 2012.